

DESY 96-094

May 1996

# Dijet Angular Distributions in Direct and Resolved Photoproduction at HERA

ZEUS Collaboration

## Abstract

Jet photoproduction, where the two highest transverse energy ( $E_T^{jet}$ ) jets have  $E_T^{jet}$  above 6 GeV and a jet-jet invariant mass above 23 GeV, has been studied with the ZEUS detector at the HERA  $ep$  collider. Resolved and direct photoproduction samples have been separated. The cross section as a function of the angle between the jet-jet axis and the beam direction in the dijet rest frame has been measured for the two samples. The measured angular distributions differ markedly from each other. They agree with the predictions of QCD calculations, where the different angular distributions reflect the different spins of the quark and gluon exchanged in the hard subprocess.

# The ZEUS Collaboration

M. Derrick, D. Krakauer, S. Magill, D. Mikunas, B. Musgrave, J.R. Okrasinski, J. Repond,  
R. Stanek, R.L. Talaga, H. Zhang

*Argonne National Laboratory, Argonne, IL, USA <sup>p</sup>*

M.C.K. Mattingly

*Andrews University, Berrien Springs, MI, USA*

G. Bari, M. Basile, L. Bellagamba, D. Boscherini, A. Bruni, G. Bruni, P. Bruni, G. Cara  
Romeo, G. Castellini<sup>1</sup>, L. Cifarelli<sup>2</sup>, F. Cindolo, A. Contin, M. Corradi, I. Gialas, P. Giusti,  
G. Iacobucci,

G. Laurenti, G. Levi, A. Margotti, T. Massam, R. Nania, F. Palmonari, A. Polini, G. Sartorelli,  
Y. Zamora Garcia<sup>3</sup>, A. Zichichi

*University and INFN Bologna, Bologna, Italy <sup>f</sup>*

C. Amelung, A. Bornheim, J. Crittenden, R. Deffner, T. Doeker<sup>4</sup>, M. Eckert, L. Feld, A. Frey<sup>5</sup>,  
M. Geerts, M. Grothe, H. Hartmann, K. Heinloth, L. Heinz, E. Hilger, H.-P. Jakob, U.F. Katz,  
S. Mengel<sup>6</sup>, E. Paul, M. Pfeiffer, Ch. Rembser, D. Schramm<sup>7</sup>, J. Stamm, R. Wedemeyer

*Physikalisches Institut der Universität Bonn, Bonn, Germany <sup>c</sup>*

S. Campbell-Robson, A. Cassidy, W.N. Cottingham, N. Dyce, B. Foster, S. George, M.E. Hayes,  
G.P. Heath, H.F. Heath, D. Piccioni, D.G. Roff, R.J. Tapper, R. Yoshida

*H.H. Wills Physics Laboratory, University of Bristol, Bristol, U.K. <sup>o</sup>*

M. Arneodo<sup>8</sup>, R. Ayad, M. Capua, A. Garfagnini, L. Iannotti, M. Schioppa, G. Susinno  
*Calabria University, Physics Dept.and INFN, Cosenza, Italy <sup>f</sup>*

A. Caldwell<sup>9</sup>, N. Cartiglia, Z. Jing, W. Liu, J.A. Parsons, S. Ritz<sup>10</sup>, F. Sciulli, P.B. Straub,  
L. Wai<sup>11</sup>, S. Yang<sup>12</sup>, Q. Zhu

*Columbia University, Nevis Labs., Irvington on Hudson, N.Y., USA <sup>q</sup>*

P. Borzemski, J. Chwastowski, A. Eskreys, Z. Jakubowski, M.B. Przybycień, M. Zachara,  
L. Zawiejski

*Inst. of Nuclear Physics, Cracow, Poland <sup>j</sup>*

L. Adamczyk, B. Bednarek, K. Jeleń, D. Kisielewska, T. Kowalski, M. Przybycień, E. Rulikowska-  
Zarębska, L. Suszycki, J. Zając

*Faculty of Physics and Nuclear Techniques, Academy of Mining and Metallurgy, Cracow, Poland <sup>j</sup>*

Z. Duliński, A. Kotański

*Jagellonian Univ., Dept. of Physics, Cracow, Poland <sup>k</sup>*

G. Abbiendi<sup>13</sup>, L.A.T. Bauerdick, U. Behrens, H. Beier, J.K. Bienlein, G. Cases, O. Deppe, K. Desler, G. Drews, M. Flasiński<sup>14</sup>, D.J. Wilkinson, C. Glasman, P. Göttlicher, J. Große-Knetter, T. Haas, W. Hain, D. Hasell, H. Heßling, Y. Iga, K.F. Johnson<sup>15</sup>, P. Joos, M. Kase-  
mann, R. Klanner, W. Koch, U. Kötz, H. Kowalski, J. Labs, A. Ladage, B. Löhr, M. Löwe,  
D. Lüke, J. Mainusch<sup>16</sup>, O. Mańczak, J. Milewski, T. Monteiro<sup>17</sup>, J.S.T. Ng, D. Notz, K. Ohren-  
berg, K. Piotrkowski, M. Roco, M. Rohde, J. Roldán, U. Schneekloth, W. Schulz, F. Selonke,  
B. Surrow, T. Voß, D. Westphal, G. Wolf, U. Wollmer,  
C. Youngman, W. Zeuner

*Deutsches Elektronen-Synchrotron DESY, Hamburg, Germany*

H.J. Grabosch, A. Kharchilava<sup>18</sup>, S.M. Mari<sup>19</sup>, A. Meyer, S. Schlenstedt, N. Wulff  
*DESY-IfH Zeuthen, Zeuthen, Germany*

G. Barbagli, E. Gallo, P. Pelfer  
*University and INFN, Florence, Italy <sup>f</sup>*

G. Maccarrone, S. De Pasquale, L. Votano  
*INFN, Laboratori Nazionali di Frascati, Frascati, Italy <sup>f</sup>*

A. Bamberger, S. Eisenhardt, T. Trefzger<sup>20</sup>, S. Wölffe  
*Fakultät für Physik der Universität Freiburg i.Br., Freiburg i.Br., Germany <sup>c</sup>*

J.T. Bromley, N.H. Brook, P.J. Bussey, A.T. Doyle, D.H. Saxon, L.E. Sinclair, M.L. Utey,  
A.S. Wilson  
*Dept. of Physics and Astronomy, University of Glasgow, Glasgow, U.K. <sup>o</sup>*

A. Dannemann, U. Holm, D. Horstmann, R. Sinkus, K. Wick  
*Hamburg University, I. Institute of Exp. Physics, Hamburg, Germany <sup>c</sup>*

B.D. Burow<sup>21</sup>, L. Hagge<sup>16</sup>, E. Lohrmann, G. Poelz, W. Schott, F. Zetsche  
*Hamburg University, II. Institute of Exp. Physics, Hamburg, Germany <sup>c</sup>*

T.C. Bacon, N. Brümmer, I. Butterworth, V.L. Harris, G. Howell, B.H.Y. Hung, L. Lamberti<sup>22</sup>,  
K.R. Long, D.B. Miller, N. Pavel, A. Prinias<sup>23</sup>, J.K. Sedgbeer, D. Sideris, A.F. Whitfield  
*Imperial College London, High Energy Nuclear Physics Group, London, U.K. <sup>o</sup>*

U. Mallik, M.Z. Wang, S.M. Wang, J.T. Wu  
*University of Iowa, Physics and Astronomy Dept., Iowa City, USA <sup>p</sup>*

P. Cloth, D. Filges  
*Forschungszentrum Jülich, Institut für Kernphysik, Jülich, Germany*

S.H. An, G.H. Cho, B.J. Ko, S.B. Lee, S.W. Nam, H.S. Park, S.K. Park  
*Korea University, Seoul, Korea <sup>h</sup>*

S. Kartik, H.-J. Kim, R.R. McNeil, W. Metcalf, V.K. Nadendla  
*Louisiana State University, Dept. of Physics and Astronomy, Baton Rouge, LA, USA <sup>p</sup>*

F. Barreiro, J.P. Fernandez, R. Graciani, J.M. Hernández, L. Hervás, L. Labarga, M. Martinez,  
J. del Peso, J. Puga, J. Terron, J.F. de Trocóniz  
*Univer. Autónoma Madrid, Depto de Física Teórica, Madrid, Spain <sup>n</sup>*

F. Corriveau, D.S. Hanna, J. Hartmann, L.W. Hung, J.N. Lim, C.G. Matthews<sup>24</sup>, P.M. Patel, M. Riveline, D.G. Stairs, M. St-Laurent, R. Ullmann, G. Zacek<sup>24</sup>

*McGill University, Dept. of Physics, Montréal, Québec, Canada*<sup>a, b</sup>

T. Tsurugai

*Meiji Gakuin University, Faculty of General Education, Yokohama, Japan*

V. Bashkirov, B.A. Dolgoshein, A. Stifutkin

*Moscow Engineering Physics Institute, Moscow, Russia*<sup>l</sup>

G.L. Bashindzhagyan<sup>25</sup>, P.F. Ermolov, L.K. Gladilin, Yu.A. Golubkov, V.D. Kobrin, I.A. Korzhavina, V.A. Kuzmin, O.Yu. Lukina, A.S. Proskuryakov, A.A. Savin, L.M. Shcheglova, A.N. Solomin, N.P. Zotov

*Moscow State University, Institute of Nuclear Physics, Moscow, Russia*<sup>m</sup>

M. Botje, F. Chlebana, J. Engelen, M. de Kamps, P. Kooijman, A. Kruse, A. van Sighem, H. Tiecke, W. Verkerke, J. Vosseveld, M. Vreeswijk, L. Wiggers, E. de Wolf, R. van Woudenberg<sup>26</sup>  
*NIKHEF and University of Amsterdam, Netherlands*<sup>i</sup>

D. Acosta, B. Bylsma, L.S. Durkin, J. Gilmore, C. Li, T.Y. Ling, P. Nylander, I.H. Park, T.A. Romanowski<sup>27</sup>

*Ohio State University, Physics Department, Columbus, Ohio, USA*<sup>p</sup>

D.S. Bailey, R.J. Cashmore<sup>28</sup>, A.M. Cooper-Sarkar, R.C.E. Devenish, N. Harnew, M. Lancaster<sup>29</sup>, L. Lindemann, J.D. McFall, C. Nath, V.A. Noyes<sup>23</sup>, A. Quadt, J.R. Tickner, H. Uijterwaal, R. Walczak, D.S. Waters, F.F. Wilson, T. Yip

*Department of Physics, University of Oxford, Oxford, U.K.*<sup>o</sup>

A. Bertolin, R. Brugnera, R. Carlin, F. Dal Corso, M. De Giorgi, U. Dosselli, S. Limentani, M. Morandin, M. Posocco, L. Stanco, R. Stroili, C. Voci, F. Zuin

*Dipartimento di Fisica dell' Università and INFN, Padova, Italy*<sup>f</sup>

J. Bulmahn, R.G. Feild<sup>30</sup>, B.Y. Oh, J.J. Whitmore

*Pennsylvania State University, Dept. of Physics, University Park, PA, USA*<sup>q</sup>

G. D'Agostini, G. Marini, A. Nigro, E. Tassi

*Dipartimento di Fisica, Univ. 'La Sapienza' and INFN, Rome, Italy*<sup>f</sup>

J.C. Hart, N.A. McCubbin, T.P. Shah

*Rutherford Appleton Laboratory, Chilton, Didcot, Oxon, U.K.*<sup>o</sup>

E. Barberis, T. Dubbs, C. Heusch, M. Van Hook, W. Lockman, J.T. Rahn, H.F.-W. Sadrozinski, A. Seiden, D.C. Williams

*University of California, Santa Cruz, CA, USA*<sup>p</sup>

J. Biltzinger, R.J. Seifert, O. Schwarzer, A.H. Walenta

*Fachbereich Physik der Universität-Gesamthochschule Siegen, Germany*<sup>c</sup>

H. Abramowicz, G. Briskin, S. Dagan<sup>31</sup>, A. Levy<sup>25</sup>

*School of Physics, Tel-Aviv University, Tel Aviv, Israel*<sup>e</sup>

J.I. Fleck<sup>32</sup>, M. Inuzuka, T. Ishii, M. Kuze, S. Mine, M. Nakao, I. Suzuki, K. Tokushuku, K. Umemori, S. Yamada, Y. Yamazaki

*Institute for Nuclear Study, University of Tokyo, Tokyo, Japan*<sup>g</sup>

M. Chiba, R. Hamatsu, T. Hirose, K. Homma, S. Kitamura<sup>33</sup>, T. Matsushita, K. Yamauchi  
*Tokyo Metropolitan University, Dept. of Physics, Tokyo, Japan*<sup>g</sup>

R. Cirio, M. Costa, M.I. Ferrero, S. Maselli, C. Peroni, R. Sacchi, A. Solano, A. Staiano  
*Universita di Torino, Dipartimento di Fisica Sperimentale and INFN, Torino, Italy*<sup>f</sup>

M. Dardo

*II Faculty of Sciences, Torino University and INFN - Alessandria, Italy*<sup>f</sup>

D.C. Bailey, F. Benard, M. Brkic, C.-P. Fagerstroem, G.F. Hartner, K.K. Joo, G.M. Levman, J.F. Martin, R.S. Orr, S. Polenz, C.R. Sampson, D. Simmons, R.J. Teuscher

*University of Toronto, Dept. of Physics, Toronto, Ont., Canada*<sup>a</sup>

J.M. Butterworth, C.D. Catterall, T.W. Jones, P.B. Kaziewicz, J.B. Lane, R.L. Saunders, J. Shulman, M.R. Sutton

*University College London, Physics and Astronomy Dept., London, U.K.*<sup>o</sup>

B. Lu, L.W. Mo

*Virginia Polytechnic Inst. and State University, Physics Dept., Blacksburg, VA, USA*<sup>q</sup>

W. Bogusz, J. Ciborowski, J. Gajewski, G. Grzelak<sup>34</sup>, M. Kasprzak, M. Krzyżanowski, K. Muchorowski<sup>35</sup>, R.J. Nowak, J.M. Pawlak, T. Tymieniecka, A.K. Wróblewski, J.A. Zakrzewski, A.F. Żarnecki

*Warsaw University, Institute of Experimental Physics, Warsaw, Poland*<sup>j</sup>

M. Adamus

*Institute for Nuclear Studies, Warsaw, Poland*<sup>j</sup>

C. Coldewey, Y. Eisenberg<sup>31</sup>, D. Hochman, U. Karshon<sup>31</sup>, D. Revel<sup>31</sup>, D. Zer-Zion

*Weizmann Institute, Nuclear Physics Dept., Rehovot, Israel*<sup>d</sup>

W.F. Badgett, J. Breitweg, D. Chapin, R. Cross, S. Dasu, C. Foudas, R.J. Loveless, S. Mattingly, D.D. Reeder, S. Silverstein, W.H. Smith, A. Vaiciulis, M. Wodarczyk

*University of Wisconsin, Dept. of Physics, Madison, WI, USA*<sup>p</sup>

S. Bhadra, M.L. Cardy, W.R. Frisken, M. Khakzad, W.N. Murray, W.B. Schmidke  
*York University, Dept. of Physics, North York, Ont., Canada*<sup>a 1</sup> also at IROE Florence, Italy  
<sup>2</sup> now at Univ. of Salerno and INFN Napoli, Italy  
<sup>3</sup> supported by Worldlab, Lausanne, Switzerland  
<sup>4</sup> now as MINERVA-Fellow at Tel-Aviv University  
<sup>5</sup> now at Univ. of California, Santa Cruz  
<sup>6</sup> now at VDI-Technologiezentrum Düsseldorf  
<sup>7</sup> now at Commasoft, Bonn  
<sup>8</sup> also at University of Torino and Alexander von Humboldt Fellow  
<sup>9</sup> Alexander von Humboldt Fellow  
<sup>10</sup> Alfred P. Sloan Foundation Fellow  
<sup>11</sup> now at University of Washington, Seattle  
<sup>12</sup> now at California Institute of Technology, Los Angeles  
<sup>13</sup> supported by an EC fellowship number ERBFMBICT 950172  
<sup>14</sup> now at Inst. of Computer Science, Jagellonian Univ., Cracow  
<sup>15</sup> visitor from Florida State University  
<sup>16</sup> now at DESY Computer Center  
<sup>17</sup> supported by European Community Program PRAXIS XXI  
<sup>18</sup> now at Univ. de Strasbourg  
<sup>19</sup> present address: Dipartimento di Fisica, Univ. “La Sapienza”, Rome  
<sup>20</sup> now at ATLAS Collaboration, Univ. of Munich  
<sup>21</sup> also supported by NSERC, Canada  
<sup>22</sup> supported by an EC fellowship  
<sup>23</sup> PPARC Post-doctoral Fellow  
<sup>24</sup> now at Park Medical Systems Inc., Lachine, Canada  
<sup>25</sup> partially supported by DESY  
<sup>26</sup> now at Philips Natlab, Eindhoven, NL  
<sup>27</sup> now at Department of Energy, Washington  
<sup>28</sup> also at University of Hamburg, Alexander von Humboldt Research Award  
<sup>29</sup> now at Lawrence Berkeley Laboratory, Berkeley  
<sup>30</sup> now at Yale University, New Haven, CT  
<sup>31</sup> supported by a MINERVA Fellowship  
<sup>32</sup> supported by the Japan Society for the Promotion of Science (JSPS)  
<sup>33</sup> present address: Tokyo Metropolitan College of Allied Medical Sciences, Tokyo 116, Japan  
<sup>34</sup> supported by the Polish State Committee for Scientific Research, grant No. 2P03B09308  
<sup>35</sup> supported by the Polish State Committee for Scientific Research, grant No. 2P03B09208

- <sup>a</sup> supported by the Natural Sciences and Engineering Research Council of Canada (NSERC)
- <sup>b</sup> supported by the FCAR of Québec, Canada
- <sup>c</sup> supported by the German Federal Ministry for Education and Science, Research and Technology (BMBF), under contract numbers 056BN19I, 056FR19P, 056HH19I, 056HH29I, 056SI79I
- <sup>d</sup> supported by the MINERVA Gesellschaft für Forschung GmbH, the Israel Academy of Science and the U.S.-Israel Binational Science Foundation
- <sup>e</sup> supported by the German Israeli Foundation, and by the Israel Academy of Science
- <sup>f</sup> supported by the Italian National Institute for Nuclear Physics (INFN)
- <sup>g</sup> supported by the Japanese Ministry of Education, Science and Culture (the Monbusho) and its grants for Scientific Research
- <sup>h</sup> supported by the Korean Ministry of Education and Korea Science and Engineering Foundation
- <sup>i</sup> supported by the Netherlands Foundation for Research on Matter (FOM)
- <sup>j</sup> supported by the Polish State Committee for Scientific Research, grants No. 115/E-343/SPUB/P03/109/95, 2P03B 244 08p02, p03, p04 and p05, and the Foundation for Polish-German Collaboration (proj. No. 506/92)
- <sup>k</sup> supported by the Polish State Committee for Scientific Research (grant No. 2 P03B 083 08) and Foundation for Polish-German Collaboration
- <sup>l</sup> partially supported by the German Federal Ministry for Education and Science, Research and Technology (BMBF)
- <sup>m</sup> supported by the German Federal Ministry for Education and Science, Research and Technology (BMBF), and the Fund of Fundamental Research of Russian Ministry of Science and Education and by INTAS-Grant No. 93-63
- <sup>n</sup> supported by the Spanish Ministry of Education and Science through funds provided by CICYT
- <sup>o</sup> supported by the Particle Physics and Astronomy Research Council
- <sup>p</sup> supported by the US Department of Energy
- <sup>q</sup> supported by the US National Science Foundation

# 1 Introduction

Jet photoproduction at HERA has been used to investigate various aspects of quantum chromodynamics (QCD) and the structure of the photon and the proton [1–6]. QCD calculations of jet cross sections can be factorized into two parts: the parton distributions in the beam particles and the matrix elements of the partonic hard scattering. The selection of the kinematic region and variables in which dijet cross sections are studied can enhance the sensitivity of the data either to the matrix elements or to the parton distributions.

In a previous analysis [6] dijet cross sections were measured in the regime where the difference between the pseudorapidities<sup>1</sup> of the two jets of highest transverse energy ( $E_T^{jet}$ ) is small ( $|\eta^{jet1} - \eta^{jet2}| < 0.5$ ). This constrained  $\theta^*$ , the angle between the jet-jet axis and the beam axis in the dijet centre of mass system, to be close to  $90^\circ$ . The cross section as a function of  $\bar{\eta} = (\eta^{jet1} + \eta^{jet2})/2$  was then sensitive to the parton distributions in the photon and proton. In contrast, in the present analysis a cut is made on  $\bar{\eta}$ , resulting in a  $\cos\theta^*$  distribution which is sensitive to the parton dynamics. The variable  $\cos\theta^*$  is calculated as

$$\cos\theta^* = \tanh\left(\frac{\eta^{jet1} - \eta^{jet2}}{2}\right). \quad (1)$$

Only the absolute value of  $\cos\theta^*$  can be determined because the outgoing jets are indistinguishable. Measuring the distribution in  $\cos\theta^*$  is preferable to measuring the jet pseudorapidity distribution because  $\cos\theta^*$  is approximately invariant under the different boosts along the beam axis arising from the spectrum of incoming parton momenta. This minimizes the sensitivity of the cross section to the momentum density distribution of the partons in the beam particles.

In leading order (LO) QCD, two types of processes lead to the photoproduction of jets. In direct processes (Fig.1a) the photon participates in the hard scatter via either boson-gluon fusion or QCD Compton scattering. These processes involve a quark propagator in the  $s$ ,  $t$  or  $u$  channel, with  $t$  and  $u$  channel processes dominating. In resolved processes (Fig.1b) the photon acts as a source of quarks and gluons, and only a fraction of its momentum participates in the hard scatter. In this case the dominant subprocesses, e.g.  $qg \rightarrow qg$ ,  $gg \rightarrow gg$  and  $qq \rightarrow qq$ , have  $t$ -channel gluon exchange diagrams. The angular dependence of the cross section for resolved processes with a spin-1 gluon propagator is approximately  $\propto (1 - |\cos\theta^*|)^{-2}$  (as in Rutherford scattering). This cross section rises more steeply with increasing  $|\cos\theta^*|$  than that for direct processes with a spin- $\frac{1}{2}$  quark propagator, where the angular dependence is approximately  $\propto (1 - |\cos\theta^*|)^{-1}$ . After inclusion of all LO diagrams, QCD predicts that the angular distribution of the outgoing partons in resolved processes will be enhanced at high  $|\cos\theta^*|$  with respect to direct photon processes. This property is expected to be preserved in next-to-leading order (NLO) calculations [7]. In addition to depending upon the incoming flux of partons, this prediction is sensitive to the relative colour factors for each subprocess and to the spins of the quark and the gluon.

The separation between direct and resolved photoproduction is only well defined at LO. To be able to make a measurement which can be compared to calculations at any order, the variable

---

<sup>1</sup> $\eta = -\ln(\tan \frac{\theta}{2})$  where  $\theta$  is the polar angle with respect to the  $z$  axis, which in the ZEUS coordinate system is defined to be the proton direction.



$x_\gamma^{OBS}$  is used to define these two kinematic regions [6]. The variable  $x_\gamma^{OBS}$  is the fraction of the photon energy contributing to the production of the two highest  $E_T^{jet}$  jets. It is defined as

$$x_\gamma^{OBS} = \frac{E_T^{jet1} e^{-\eta^{jet1}} + E_T^{jet2} e^{-\eta^{jet2}}}{2E_\gamma} \quad (2)$$

where  $E_\gamma$  is the initial photon energy. Direct processes as defined at leading order have high  $x_\gamma^{OBS}$  since all the photon's energy participates in the production of the hard jets, while resolved processes as defined at leading order have low  $x_\gamma^{OBS}$  since part of the photon's energy goes into the photon remnant. Thus the different spins of the quark and gluon propagators that are dominant in the high  $x_\gamma^{OBS}$  and the low  $x_\gamma^{OBS}$  processes respectively should be reflected in the  $\cos\theta^*$  distributions of the two samples. Henceforth throughout the following, in both the data and the calculations, direct and resolved samples are defined in terms of a cut on  $x_\gamma^{OBS}$  rather than in terms of the LO diagrams, unless explicitly stated otherwise.

Measurements of dijet angular distributions in  $p\bar{p}$  events have shown good agreement with the predictions of perturbative QCD [8] in both fermionic and bosonic exchange processes [9]. The measurement presented here tests QCD in a different kinematic regime and in a different process, and provides an opportunity to study the parton dynamics of two distinct dijet production mechanisms in the same experiment.

## 2 Experimental Setup

In 1994 HERA provided 820 GeV protons and 27.5 GeV positrons colliding in 153 bunches. Additional unpaired positron and proton bunches circulated to allow monitoring of the background from beam-gas interactions. Events from empty bunches were used to estimate the background from cosmic rays. The total integrated luminosity used in this analysis is  $2.6 \text{ pb}^{-1}$  collected during this running period.

Details of the ZEUS detector have been described elsewhere [10]. The primary components used in this analysis are the central calorimeter and the central tracking detectors. The uranium-scintillator calorimeter [11] covers 99.7% of the total solid angle and is subdivided into three parts, forward (FCAL) covering  $4.3 > \eta > 1.1$ , barrel (BCAL) covering the central region  $1.1 > \eta > -0.75$  and rear (RCAL) covering the backward region  $-0.75 > \eta > -3.8$  for an event at the nominal interaction point. Each part consists of an electromagnetic section followed by a hadronic section, with cell sizes of approximately  $5 \times 20 \text{ cm}^2$  ( $10 \times 20 \text{ cm}^2$  in the rear calorimeter) and  $20 \times 20 \text{ cm}^2$  respectively. The central tracking system consists of a vertex detector [12] and a central tracking chamber [13] enclosed in a 1.43 T solenoidal magnetic field. A lead-scintillator photon calorimeter is used to measure the luminosity via the positron proton Bremsstrahlung process. This calorimeter is installed 100 m along the HERA tunnel from the interaction point in the positron direction and subtends a small angle at the interaction vertex [14]. Positrons scattered through small angles are detected in a similar lead-scintillator calorimeter.

### 3 Event Selection

The ZEUS detector uses a three level trigger system. At the first level events were triggered on a coincidence of a regional or transverse energy sum in the calorimeter and a track from the interaction point measured in the central tracking chamber. At the second level at least 8 GeV total transverse energy, excluding the eight calorimeter towers immediately surrounding the forward beampipe, was required, and cuts on calorimeter energies and timing were used to suppress events caused by interactions between the proton beam and residual gas in the beam pipe [15]. At the third level, jets were found using the calorimeter cell energies and positions as input to a cone algorithm[16]. Events were required to have at least two jets of  $E_T^{jet} > 3.5$  GeV and  $\eta^{jet} < 3.0$ . Additional tracking cuts were made to reject proton beam-gas interactions and cosmic ray events.

Further cuts are applied offline. Charged current events are rejected by a cut on the missing transverse momentum measured in the calorimeter. To reject remaining beam-gas and cosmic ray background events, tighter cuts using the final vertex position, other tracking information and timing information are applied. Two additional cuts are made [4], based upon different measurements of the inelasticity, defined in the ZEUS frame as  $y = 1 - \frac{E'_e}{2E_e}(1 - \cos \theta'_e)$  where  $E_e$  is the energy of the incoming positron and  $E'_e$  and  $\theta'_e$  are the energy and polar angle of the outgoing positron.

1. Events with a positron candidate in the uranium calorimeter are removed if  $y_e < 0.7$ , where  $y_e$  is the value of  $y$  as measured assuming the positron candidate is the scattered positron.
2. A cut is made on the Jacquet-Blondel measurement of  $y$  [17],  $y_{JB} = \sum_i (E_i - E_{zi})/2E_e$ , where  $E_{zi} = E_i \cos \theta_i$ , and  $E_i$  is the energy deposited in the calorimeter cell  $i$  which has a polar angle  $\theta_i$  with respect to the measured  $z$ -vertex of the event. The sum runs over all calorimeter cells. For any event where the scattered positron entered the uranium calorimeter and either was not identified or gave  $y_e$  above 0.7, the value of  $y_{JB}$  will be near to one. Proton beam-gas events will have low values of  $y_{JB}$ . To further reduce the contamination from both these sources, it is required that  $0.15 < y_{JB} < 0.7$ . This range corresponds to the true  $y$  range of  $0.25 < y < 0.8$ .

These cuts restrict the range of the photon virtuality to less than  $\sim 4 \text{ GeV}^2$ , with a median of around  $10^{-3} \text{ GeV}^2$ , which excludes deep inelastic scattering (DIS) events.

To select dijet candidates, a cone algorithm is applied to the calorimeter cells using a cone radius  $R = \sqrt{(\delta\phi)^2 + (\delta\eta)^2} = 1$ , where  $\delta\eta(\delta\phi)$  is the distance in  $\eta(\phi)$  of the centre of a calorimeter cell from the jet centre. The jet energy measured in the ZEUS detector has been corrected using the Monte Carlo(MC) events described in the next section. The energy response of the ZEUS calorimeter is estimated by comparing jets found in the hadronic final state of the MC generator to jets found in the simulated detector. The average shift in jet energies is  $-17\%$  and varies between  $-10\%$  and  $-25\%$  depending upon  $\eta^{jet}$ . The description of the jet energy shift in the MC has been checked using tracking and the incident photon energy deduced from the

energy of the electron which is measured in the small-angle electron tagger. This description is accurate to within 5% [5, 6]. After this correction, events are required to have at least two jets with  $E_T^{jet} \geq 6$  GeV and  $\eta^{jet} < 2.5$ . For events with three or more jets, the two highest  $E_T^{jet}$  jets are used to calculate all jet-related event properties. This procedure is also employed later in all the theoretical and MC predictions shown.

For a given centre-of-mass energy, events at high  $|\cos \theta^*|$  have smaller scattering angles and thus lower  $E_T^{jet}$ . In order to study the  $|\cos \theta^*|$  distribution up to  $|\cos \theta^*| = 0.85$  without bias from the  $E_T^{jet}$  requirement, a cut of  $M_{jj} > 23$  GeV has been applied.  $M_{jj}$  is the dijet invariant mass calculated using the relationship

$$M_{jj} = \sqrt{2E_T^{jet1} E_T^{jet2} [\cosh(\eta^{jet1} - \eta^{jet2}) - \cos(\phi^{jet1} - \phi^{jet2})]}, \quad (3)$$

where  $\phi^{jet}$  is the azimuthal angle of the jet in the HERA frame. For two jets back-to-back in  $\phi$  and with equal  $E_T^{jet}$ ,  $M_{jj} \approx 2E_T^{jet} / \sqrt{1 - |\cos \theta^*|^2}$ .

Because of the asymmetric beam energies, the two parton centre-of-mass system is typically boosted to the forward direction. For resolved photon processes, this effect is bigger because only a fraction of the photon's momentum participates in the hard scatter. MC simulations show that as a result, a significant fraction of jets are at rapidities ( $\eta > 2.5$ ) where they are not well measured in the ZEUS detector. To remove this bias, a cut  $|\bar{\eta}| < 0.5$  was applied, where  $\bar{\eta}$ , the average  $\eta$  of the two jets, is a measure of the boost of the dijet scattering system in the HERA frame:

$$\bar{\eta} \approx \eta_{boost} = \frac{1}{2} \ln \left( \frac{E_p x_p}{E_\gamma x_\gamma} \right) \quad (4)$$

where  $x_p$  and  $x_\gamma$  are the momentum fractions of the incoming partons in the proton and photon respectively and  $E_p$  is the incoming proton energy. In a simple (LO)  $2 \rightarrow 2$  scatter, the dijet invariant mass is related to  $x_p$  and  $x_\gamma$  by

$$M_{jj} = \sqrt{4E_\gamma E_p x_\gamma x_p} = \sqrt{4E_e E_p y x_\gamma x_p}. \quad (5)$$

The requirement that the dijet system has high mass and small boost selects events with  $\gamma p$  centre-of-mass energies mostly above 190 GeV, and suppresses events with low  $x_\gamma^{OBS}$ . Thus the incoming partons have approximately equal and opposite momenta and energies sufficient to produce dijets in a region of good acceptance for a wide range of scattering angles. In the range of  $x_\gamma$  and  $x_p$  selected by these cuts the photon and proton parton distributions are fairly well determined by previous measurements [3, 5, 6, 15, 18].

After these cuts a total of 4964 events remain with  $|\cos \theta^*| < 0.85$ , of which 1982 have  $x_\gamma^{OBS} < 0.75$  and 2982 have  $x_\gamma^{OBS} \geq 0.75$ . Events with a third jet which passes the  $E_T^{jet}$  and  $\eta^{jet}$  cuts comprise 9% of the final sample. 21% of all events have their scattered positrons detected in the small-angle tagger, as is expected for photoproduction events [5]. The beam-gas background, measured using unpaired bunches, is less than 1%. The contamination from events with photon virtualities greater than 4 GeV<sup>2</sup> is estimated to be 3.3% using simulated deep inelastic scattering (DIS) events.

## 4 Results and Discussion

In Fig.2 the ZEUS dijet data (black dots) are compared to the results of two QCD MC simulation programs, HERWIG58 [19] (solid lines) and PYTHIA57 [20] (broken lines). The GRV [21] parton distributions are used for the photon and the MRSA [22] parton distributions are used for the proton. The simulation programs are based on LO QCD calculations for the hard scatter and include parton showering and hadronization effects. The minimum transverse momentum of the hard scatter is set to 2.5 GeV. For both programs the direct and resolved photon processes are generated separately and combined according to the ratio of their generated cross sections. The combined MC distributions are then normalized to the number of data events. In the case of HERWIG resolved processes, multiparton interactions are included [23], as this has been shown to improve the simulation of the energy flow around the jet axis in low- $M_{jj}$  events [24]. All the MC events are passed through a detailed simulation of the ZEUS detector and the same jet energy correction procedure as was applied to the data. Fig.2a shows the distribution of events in  $E_T^{jet}$ , which falls steeply with increasing  $E_T^{jet}$ . At low  $E_T^{jet}$  the dijet mass cut causes the distribution to turn over. Fig.2b shows the  $M_{jj}$  distribution, which falls steeply with increasing  $M_{jj}$  and extends to masses of 60 GeV. The  $\bar{\eta}$  distribution is shown in Fig.2c, and rises with increasing  $\bar{\eta}$  due to the asymmetric momenta of the photon and proton. The  $\bar{\eta}$  cut leads to an  $\eta^{jet}$  distribution which is peaked in the forward and rear directions, as shown in Fig.2d. Note also that due to the  $\bar{\eta}$  cut, the absolute value of  $\eta^{jet}$  is restricted to be below 1.8. For all these distributions the data are reasonably well described by PYTHIA and HERWIG, although HERWIG gives more jets in the central region in  $\eta^{jet}$  and at high  $E_T^{jet}$  than are seen in the data.

Fig.3a shows the uncorrected  $x_p^{OBS}$  distribution, where  $x_p^{OBS}$  is the fraction of the proton's energy contributing to the production of the two highest  $E_T^{jet}$  jets:

$$x_p^{OBS} = \frac{E_{T1}e^{\eta^{jet1}} + E_{T2}e^{\eta^{jet2}}}{2E_p}. \quad (6)$$

The events lie in the range  $0.006 < x_p^{OBS} < 0.06$ , with the most probable value at  $x_p^{OBS} \approx 0.016$ . Fig.3b shows the uncorrected  $x_\gamma^{OBS}$  distribution<sup>2</sup>. Contributions from the direct photon LO diagrams (e.g. Fig.1a) (broken line) and the resolved photon LO diagrams (e.g. Fig.1b) (dotted line) of HERWIG are shown together with the combined distribution (solid line). PYTHIA events, not shown in the figure, have a similar distribution. The data exhibit a slightly lower mean  $x_\gamma^{OBS}$  than the MC. A cut is applied at  $x_\gamma^{OBS} = 0.75$  to define the direct and resolved photon samples. The effect of the imperfect description of the data by MC on the evaluation of the cross sections is evaluated by varying the  $x_\gamma^{OBS}$  cut, and is small. The transverse energy flow around the jets is shown in Fig.3c for resolved and in Fig.3d for direct events. In this sample, which has high  $M_{jj}$  values, both the HERWIG sample with multiple interactions included and the PYTHIA sample without multiple interactions describe the jet profiles reasonably well in both direct and resolved events. The requirements of high mass and small boost remove the

---

<sup>2</sup> $x_\gamma^{OBS}$  was measured using the uncorrected jet transverse energies. This takes advantage of cancellations between energy losses in  $E_T^{jet}$  and  $E_\gamma = y_{JB}E_e$ .

disagreement in the forward energy flow between data and the simulations which has been reported elsewhere [3, 5, 6] in hard photoproduction at HERA.

The resolution of the kinematic variables has been studied by comparing in the MC simulation jets reconstructed from final state particles (hadron jets) with jets reconstructed from the energies measured in the calorimeter (calorimeter jets), and by comparing  $y_{JB}$  with the true  $y$ . The difference in  $|\cos\theta^*|$  between the hadron and detector levels has a mean of zero, a width of 0.03 and is approximately independent of  $|\cos\theta^*|$ ,  $M_{jj}$  and  $\bar{\eta}$ . The resolution of  $x_\gamma^{OBS}$  is 8.7% at  $x_\gamma^{OBS} = 0.75$ . For the variables  $E_T^{jet}$ ,  $M_{jj}$  and  $y$ , the resolutions are 13.2%, 11.1% and 11.0% respectively at the values at which the cuts are applied.

The MC samples have been used to correct for the efficiency of the trigger and selection cuts and migrations, and for the contamination from DIS events. The final bin-by-bin correction factors are approximately independent of  $|\cos\theta^*|$  and are around 1.1 for the resolved and 1.5 for the direct cross section. These correction factors are calculated as the ratio of the purity ( $= N_{\text{true,rec}}/N_{\text{rec}}$ ) to the efficiency ( $= N_{\text{true,rec}}/N_{\text{true}}$ ) in each bin.  $N_{\text{true}}$  is the number of events generated in the bin,  $N_{\text{rec}}$  is the number of events reconstructed in the bin after detector smearing and all experimental cuts, and  $N_{\text{true,rec}}$  is the number of events which were both generated in the bin and reconstructed in that bin. The difference between the correction factors for resolved and direct events is due to the fact that the  $E_T^{jet}$  and  $M_{jj}$  distributions are steeper in resolved processes than in the direct, and thus migrations from below the cuts are more significant, giving a lower purity for resolved than direct.

The sensitivity of the measured cross sections to the selection cuts has been investigated by varying the cuts on the reconstructed variables in the data and HERWIG MC samples and re-evaluating the cross section. In addition, the cross section was re-evaluated using a different ratio of the direct and resolved contributions, and using the PYTHIA sample. The systematic uncertainty arising from the subtraction of the contamination coming from DIS was estimated by using two different DIS Monte Carlo generators and two different positron-finding algorithms [15, 18]. We have also allowed for the possibility that the detector simulation may overestimate the detector energy response by up to 5%, as mentioned in section 3.

The cross sections  $d\sigma/d|\cos\theta^*|$  for  $ep \rightarrow \text{dijets} + X$  in the range  $M_{jj} > 23$  GeV,  $E_T^{jet} > 6$  GeV,  $|\bar{\eta}| < 0.5$ ,  $0.25 < y < 0.8$  and for virtualities of the exchanged photon  $< 4$  GeV<sup>2</sup> are listed in table 1. For the direct photoproduction sample the  $ep$  cross section rises from around 0.8 nb at  $|\cos\theta^*| = 0$  to around 6 nb at  $|\cos\theta^*| = 0.85$ . For the resolved photoproduction sample the  $ep$  cross section rises from around 0.2 nb at  $|\cos\theta^*| = 0$  to around 4 nb at  $|\cos\theta^*| = 0.85$ . In Fig.4a and b the two cross sections have been normalized to unity at  $|\cos\theta^*| = 0$  so that the shapes can be compared directly. To determine the normalization, the 5 lowest  $|\cos\theta^*|$  bins were fitted to the functional form expected for the dominant cross section in each sample (as described in section 1), which is slowly rising in this region. The only free parameter in this fit is the normalisation of the function. The intercept of the function then gives the factor by which the data are divided. In Fig.4a the data are compared to LO and partial <sup>3</sup> NLO QCD parton level calculations [7]. The resolved cross section is seen to rise more steeply than the direct cross section with increasing  $|\cos\theta^*|$ . There is good agreement between data and theory,

---

<sup>3</sup>The NLO calculations do not yet include terms of  $O(\alpha_s^3 \times f)$ , where  $f$  is the flux of partons in the photon.

verifying the expected effects of the spins of the quark and gluon propagators. This is also seen in Fig.4b, where the data are compared to the HERWIG and PYTHIA predictions. For both of the generators, MRSA(proton) and GRVLO(photon) [21] parton parameterisation sets are used. The MC curves were also made with different parton distribution sets in the photon and proton. The largest change seen was for the LAC1 [25] photon parton distribution set, where there is a 35% increase in the prediction in the highest  $|\cos\theta^*|$  bin. In all the calculations, resolved and direct samples are defined on the basis of the cut on  $x_\gamma^{OBS}$ , exactly as in the data. Both the MC and the parton level calculations show the same behaviour, suggesting that the effects of parton showers and hadronisation on this distribution are small. The data are in good agreement with the MC and with the calculations.

The only difference in the cuts applied to the two samples is the cut on  $x_\gamma^{OBS}$  which is used to separate the resolved and direct samples. A MC study has been performed to investigate whether the different behaviour of the two cross sections might be a kinematic effect of this cut. The study shows that the tail of the resolved photon LO diagrams (e.g. Fig.1b) which lie above  $x_\gamma^{OBS} = 0.75$  retain the steeply rising  $|\cos\theta^*|$  distribution characteristic of the low- $x_\gamma^{OBS}$  events. Thus the different behaviour of the two cross sections is due to the different partonic subprocesses which contribute in the different  $x_\gamma^{OBS}$  regions.

## 5 Summary and Conclusion

The dijet angular cross section  $d\sigma/d|\cos\theta^*|$ , where  $\theta^*$  is the jet scattering angle in the dijet c.m.s, has been measured for  $ep \rightarrow 2$  or more jets with transverse energies  $E_T^{jet} \geq 6$  GeV, dijet invariant mass  $M_{jj} > 23$  GeV and average pseudorapidity  $|\bar{\eta}| < 0.5$ , in the range  $0.25 < y < 0.8$  and for virtualities of the exchanged photon less than 4 GeV<sup>2</sup>. The cross section has been measured for resolved ( $x_\gamma^{OBS} < 0.75$ ) and direct ( $x_\gamma^{OBS} \geq 0.75$ ) processes. The angular dependence for the two samples is significantly different.

The dependence of  $d\sigma/d|\cos\theta^*|$  on  $|\cos\theta^*|$  reflects the different spins of the quark and gluon propagators and the relative contributions of the underlying subprocesses in resolved and direct photoproduction. In LO QCD the cross section rises faster with increasing  $|\cos\theta^*|$  for resolved photoproduction, where processes involving spin-1 gluon exchange dominate, than for direct photoproduction, where processes involving spin-1/2 quark exchange dominate. These expectations are preserved in NLO QCD calculations and in Monte Carlo simulations which include parton showering and hadronisation models. The  $|\cos\theta^*|$  dependence of the measured cross sections is in good agreement with these theoretical predictions and thus confirms fundamental aspects of quantum chromodynamics.

## Acknowledgements

It is a pleasure to thank the HERA accelerator group and the computing and networking support staff at DESY, without whom this analysis would not have been possible, and to thank J. Owens for providing us with his calculations. The continuing encouragement from the DESY directorate is greatly appreciated.

## References

- [1] H1 Collab., T. Ahmed et al., Phys. Lett. B297 (1992) 205.
- [2] ZEUS Collab., M. Derrick et al., Phys. Lett. B297 (1992) 404.
- [3] H1 Collab., I. Abt et al., Phys. Lett. B314 (1993) 436.
- [4] ZEUS Collab., M. Derrick et al., Phys. Lett. B322 (1994) 287.
- [5] ZEUS Collab., M. Derrick et al., Phys. Lett. B342 (1995) 417.
- [6] ZEUS Collab., M. Derrick et al., Phys. Lett. B348 (1995) 665.
- [7] H. Baer, J. Ohnemus, and J. F. Owens, Phys. Rev. D40 (1989) 2844;  
J. F. Owens, private communication.
- [8] UA1 Collab., G. Arnison et al., Phys. Lett. B136 (1984) 294;  
UA1 Collab., G. Arnison et al., Phys. Lett. B177 (1986) 244;  
CDF Collab., F. Abe et al., Phys. Rev. Lett. 62 (1989) 3020.
- [9] CDF Collab., F. Abe et al., Phys. Rev. Lett. 73 (1994) 2296.
- [10] ZEUS Collab., The ZEUS detector, Status Report (1993).
- [11] M. Derrick et al., Nucl. Instr. and Meth. A309 (1991) 77;  
A. Andresen et al., Nucl. Instr. and Meth. A309 (1991) 101;  
A. Bernstein et al., Nucl. Instr. and Meth. A336 (1993) 23.
- [12] C. Alvisi et al., Nucl. Instr. and Meth. A305 (1991) 30.
- [13] B. Foster et al., Nucl. Phys. B, Proc. Suppl. B32 (1993) 181.
- [14] J. Andruszków et al., DESY 92-066.
- [15] ZEUS Collab., M. Derrick et al., Phys. Lett. B316 (1993) 412.
- [16] J. Huth et al., Proc. of the 1990 DPF Summer Study on High Energy Physics, Snowmass, Colorado, edited by E.L. Berger (World Scientific, Singapore, 1992) p. 134;  
UA1 Collab., G. Arnison et al., Phys. Lett. 123B (1983) 115.
- [17] F. Jacquet and A. Blondel, in Proceedings of the study of an  $ep$  facility for Europe, Hamburg, ed. U. Amaldi, (DESY 79/48, 1979) 391.
- [18] ZEUS Collab., M. Derrick et al., Zeit. f. Phys. C65 (1995) 379;  
H1 Collab., T. Ahmed et al., Nucl. Phys. B439 (1995) 471;  
ZEUS Collab., M. Derrick et al., Zeit. f. Phys. C69 (1996) 607.
- [19] G. Marchesini et al., Comp. Phys. Comm. 67 (1992) 465.

- [20] H.-U. Bengtsson and T. Sjöstrand, Comp. Phys. Comm. 46 (1987) 43;  
T. Sjöstrand, CERN-TH.6488/92 (1992).
- [21] M. Glück, E. Reya and A. Vogt, Phys. Rev. D46 (1992) 1973.
- [22] A. Martin, W.J. Stirling and R.G. Roberts, Phys. Rev. D50 (1994) 6734.
- [23] T. Sjöstrand and M. van Zijl, Phys. Rev. D36 (1987) 2019;  
G. A. Schuler and T. Sjöstrand, Phys. Lett. B300 (1993) 169; Nucl. Phys. B407 (1993) 539;  
J. M. Butterworth and J. R. Forshaw, J. Phys. G19 (1993) 1657;  
J. M. Butterworth, J. R. Forshaw and M. H. Seymour, CERN-TH-95-82, to appear in Zeit. f. Phys. C.
- [24] H1 Collab., S. Aid et al., Zeit. f. Phys. C70 (1996) 17.
- [25] H. Abramowicz, K. Charchula and A. Levy, Phys. Lett. B269 (1991) 458.
- [26] CTEQ Collab., J. Botts et al., Phys. Lett. B304 (1993) 15;  
CTEQ Collab., J. Botts et al. (to be published).



$ \cos \theta^* $ range	Direct (nb / unit $ \cos \theta^* $ )				
	$d\sigma/d \cos \theta^*  \pm \text{stat.}$	syst. error	PYTHIA	E scale -5%	E scale +5%
0.000 to 0.085	$0.80 \pm 0.12$	$+0.06/-0.09$	-0.08	-0.07	0.06
0.085 to 0.170	$0.83 \pm 0.13$	$+0.07/-0.13$	-0.10	-0.13	0.11
0.170 to 0.255	$0.98 \pm 0.15$	$+0.02/-0.13$	-0.17	-0.16	0.16
0.255 to 0.340	$0.90 \pm 0.14$	$+0.02/-0.08$	-0.13	-0.12	0.12
0.340 to 0.425	$1.26 \pm 0.19$	$+0.15/-0.16$	-0.30	-0.21	0.26
0.425 to 0.510	$1.50 \pm 0.18$	$+0.08/-0.19$	-0.26	-0.26	0.24
0.510 to 0.595	$1.41 \pm 0.17$	$+0.18/-0.08$	-0.10	-0.21	0.14
0.595 to 0.680	$2.70 \pm 0.28$	$+0.36/-0.35$	-0.27	-0.53	0.51
0.680 to 0.765	$3.81 \pm 0.33$	$+0.14/-0.29$	-0.30	-0.57	0.36
0.765 to 0.850	$5.99 \pm 0.48$	$+0.81/-0.40$	-0.37	-0.96	0.86
$ \cos \theta^* $ range	Resolved (nb / unit $ \cos \theta^* $ )				
	$d\sigma/d \cos \theta^*  \pm \text{stat.}$	syst. error	PYTHIA	E scale -5%	E scale +5%
0.000 to 0.085	$0.21 \pm 0.08$	$+0.06/-0.08$	-0.09	-0.04	0.00
0.085 to 0.170	$0.23 \pm 0.12$	$+0.09/-0.12$	-0.08	-0.06	-0.02
0.170 to 0.255	$0.23 \pm 0.10$	$+0.04/-0.07$	0.01	-0.06	0.12
0.255 to 0.340	$0.28 \pm 0.09$	$+0.13/-0.02$	0.00	-0.02	0.04
0.340 to 0.425	$0.27 \pm 0.10$	$+0.10/-0.06$	-0.03	0.01	0.02
0.425 to 0.510	$0.42 \pm 0.11$	$+0.11/-0.04$	-0.03	-0.06	0.11
0.510 to 0.595	$0.77 \pm 0.17$	$+0.08/-0.08$	0.21	-0.13	0.10
0.595 to 0.680	$1.13 \pm 0.21$	$+0.16/-0.26$	-0.02	-0.22	0.07
0.680 to 0.765	$2.03 \pm 0.25$	$+0.36/-0.19$	0.01	-0.39	0.63
0.765 to 0.850	$4.31 \pm 0.43$	$+0.47/-0.39$	0.15	-0.85	0.97

Table 1: Differential cross sections  $d\sigma/d|\cos \theta^*|$  for  $ep \rightarrow 2$  or more jets with  $E_T^{jet} \geq 6$  GeV,  $M_{jj} > 23$  GeV and  $|\bar{\eta}| < 0.5$ , in the range  $0.25 < y < 0.8$  and for virtualities of the exchanged photon less than 4 GeV<sup>2</sup>, for direct and resolved processes. The first column shows the cross section and statistical errors in units of nb, the second column the uncorrelated systematic errors, the third column the shift in the cross section when the correction is evaluated using PYTHIA instead of HERWIG and the fourth and fifth columns the shifts in the cross section when the calorimeter energy calibration is varied by  $\pm 5\%$ . There is an additional overall uncertainty of 3.3% arising from the luminosity measurement.

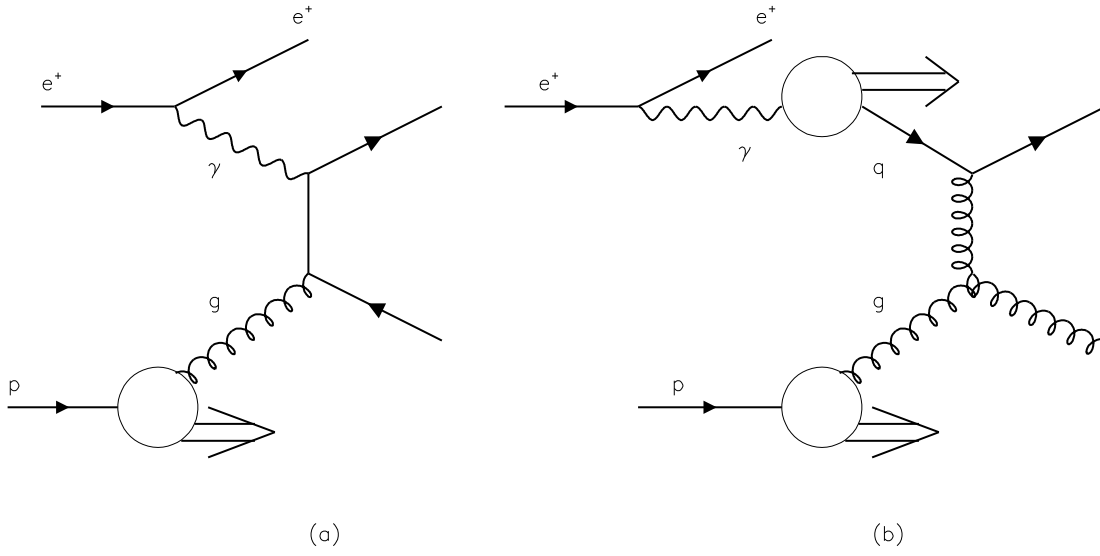


Figure 1: Examples of LO QCD (a) ‘direct’ and (b) ‘resolved’ dijet production diagrams.

# ZEUS 1994

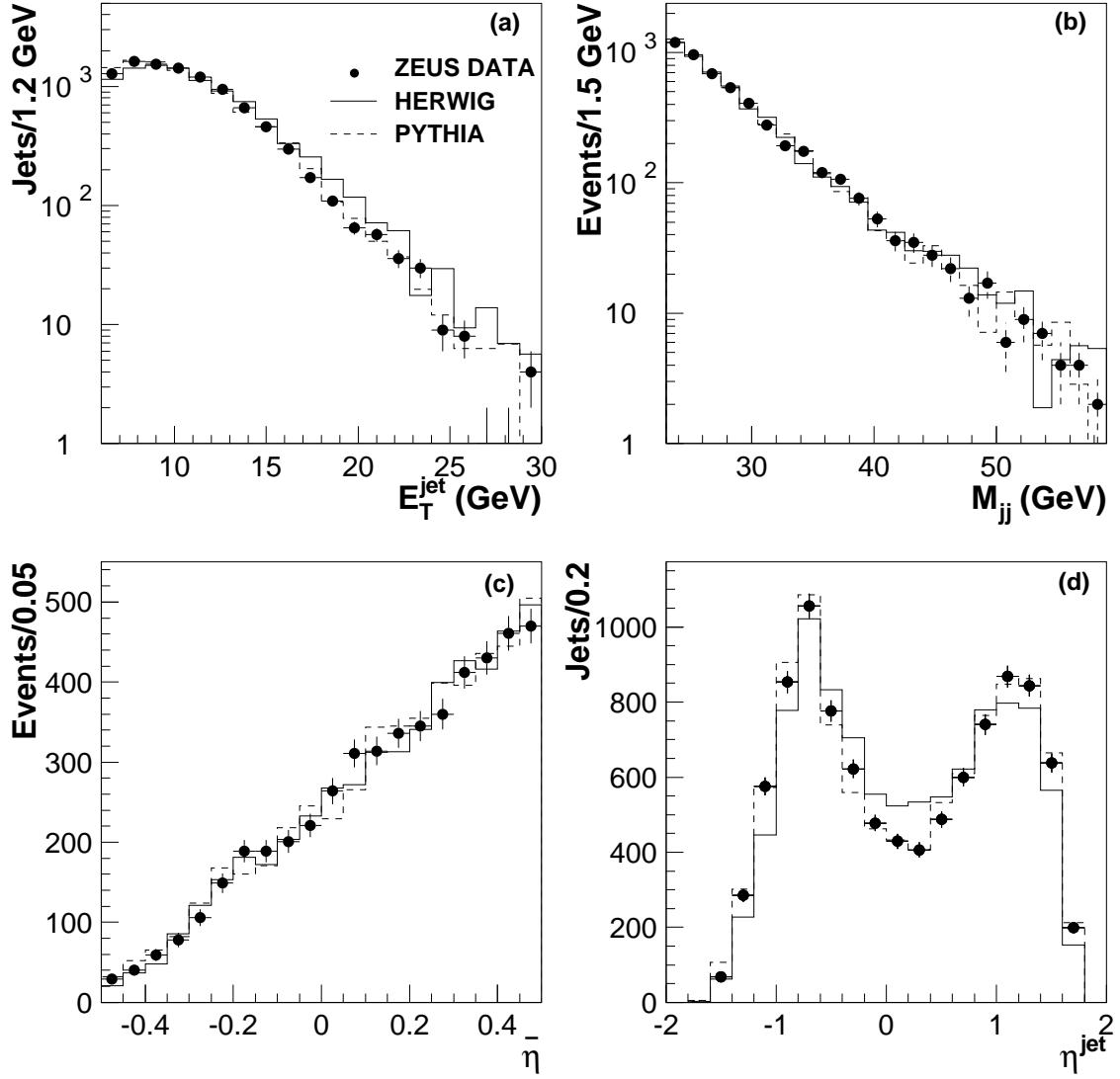


Figure 2: (a)  $E_T^{jet}$ , (b)  $M_{jj}$ , (c)  $\bar{\eta}$  and (d)  $\eta^{jet}$  distributions. Raw ZEUS data are compared to the results of the HERWIG58 (solid line) and PYTHIA57 (broken line) Monte Carlo models after simulation of all detector effects and application of selection cuts. The MC samples have been normalized to the number of events in the data. Only statistical errors are shown.

# ZEUS 1994

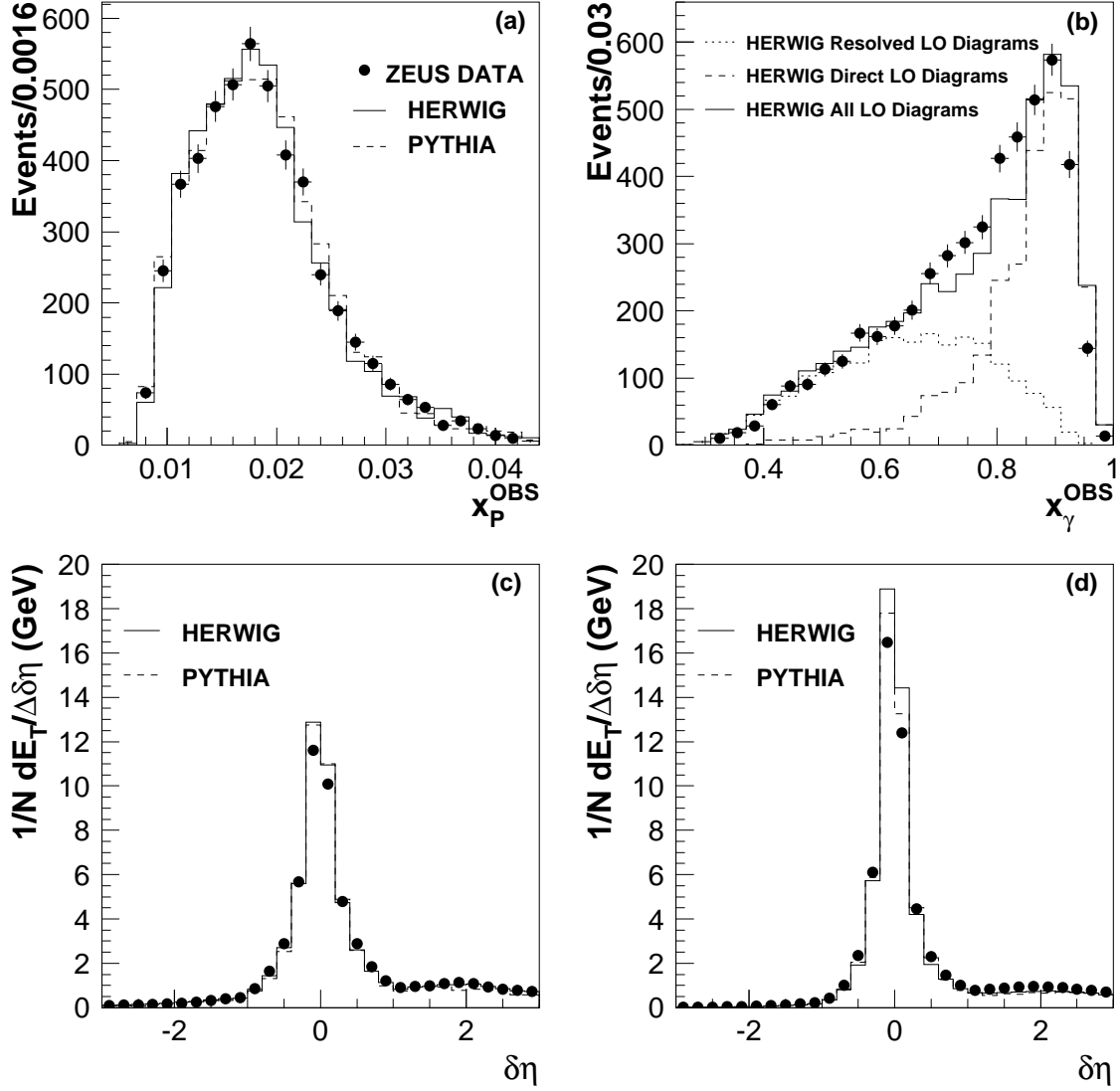


Figure 3: Raw ZEUS data compared to results of Monte Carlo models after simulation of detector effects and application of selection cuts. (a)  $x_p^{OBS}$  and (b)  $x_\gamma^{OBS}$  distribution. The MC samples have been normalized to the number of events in the data. Figures (c) and (d) show the uncorrected transverse energy flow  $1/N dE_T/d\delta\eta$  around the jet axis, for cells within one radian in  $\phi$  of the jet axis, for (c) resolved ( $x_\gamma^{OBS} < 0.75$ ), (d) direct ( $x_\gamma^{OBS} > 0.75$ ) events. Only statistical errors are shown. In (a), (c) and (d), the histograms are HERWIG58 (solid line) and PYTHIA57 (broken line). In (b), the solid line is HERWIG58, the broken line is the distribution of the LO direct diagrams (e.g. Fig.1a) and the dotted line is that of the LO resolved diagrams (e.g. Fig.1b).

# ZEUS 1994

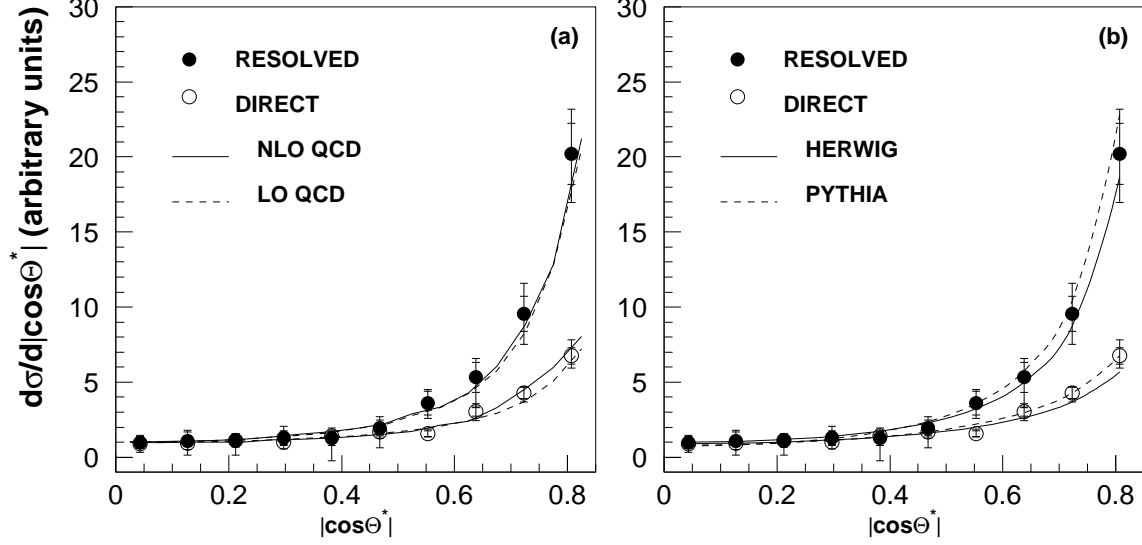


Figure 4:  $d\sigma/d|\cos\theta^*|$  normalized to one at  $\cos\theta^* = 0$  for resolved (black dots) and direct (open circles) photoproduction. In (a), the ZEUS data are compared to the NLO prediction (solid line) and the LO prediction (broken line). The parton distribution sets used in the calculation are CTEQ3M [26] for the proton and GRV (LO) [21] for the photon. In (b), the broken line is the PYTHIA distribution and solid line is HERWIG distribution. The inner error bars are the statistical errors, the outer error bars are the sum in quadrature of the statistical and systematic errors, excluding the energy scale and luminosity uncertainties (see Table 1).